Journal of Energy Storage 19 (2018) 170–184

Contents lists available at ScienceDirect

Journal of Energy Storage

journal homepage: www.elsevier.com/locate/est

Duty-cycle characterisation of large-format automotive lithium ion pouch cells for high performance vehicle applications

Quirin Kellner*, Daniel Worwood, Anup Barai, Widanalage Dhammika Widanage, James Marco

WMG, University of Warwick, Coventry, CV4 7AL, UK

ARTICLE INFO

Keywords:
High-performance
Electric vehicles
Lithium ion battery
Characterisation
Degradation

ABSTRACT

The long-term behaviour of lithium ion batteries in high-performance (HP) electric vehicle (EV) applications is not well understood due to a lack of suitable testing cycles and experimental data. As such a generic HP duty cycle (HP-C), representing driving on a race track is validated, and six NMC graphite cells are characterised with respect to cycle-life. To enable a comparison between the HP-EV environment and conventional road driving, two test groups of cells are subject to an experimental evaluation over 200 duty cycles that includes a representative HP-C and a standard duty cycle from the IEC 62660-1 standard (IECC). After testing, both test groups display increased energy capacity, increased pure Ohmic resistance, lower charge transfer resistance an extended OCV operating window. The changes are more pronounced for cells subject to the HP-C. Based on capacity tests, Electrochemical Impedance Spectroscopy (EIS), pseudo-OCV tests, and Pulse Multisine Characterisation, it is concluded that the changes in cell characteristics are most likely caused by cracking of the electrode material caused by high electrical current pulses. With continued cycling, cells cycled with the HP-C are expected to show degradation at an increased rate due to raised temperatures, and more pronounced electrode cracking.

1. Introduction

In recent years, the development and improvement of lithium ion batteries (LIBs) has underpinned the electrification of the transport sector with new markets, such as the strategically important high-performance (HP) vehicle segment, becoming a target sector for many new start-up organisations and more established original equipment manufacturers (OEMs) [1]. Currently, automotive OEMs are developing innovative electric vehicles (EVs) for this segment, with examples including the Jaguar I-PACE and Aston Martin Rapid-E, both set to launch in 2018 [2], in addition to more established vehicles such as the Tesla Model S. Challenges for the success of these vehicles are often reported to be key battery characteristics such as: Cycle life, energy capacity, power capability, degradation, safety, reliability, and cost. Notwithstanding the system integration requirements, such as packaging and thermal management that are required to realise a complete battery system [3].

Extensive research has been undertaken regarding the operation and degradation of lithium ion battery cells intended for automotive use [4,5]. One limitation of this research is that often, several studies use relatively simplistic constant current charge and discharge tests, often at different current rates and environmental temperatures as a means to estimate cycle life over a broad spectrum of operating conditions [5–7]. These tests are known to be largely unrepresentative of the day to day battery operation within an EV. Research published by Barre et al. [8] has indicated that complex electrical loading profiles result in different ageing characteristics than conventional galvanostatic profiles.

As such, more complex testing profiles are required to more accurately predict the behaviour and cycle ageing progression of cells in HP automotive use cases. A study by Barre et al. [9] investigated battery data, which was collected from a passenger EV following a predetermined driving cycle, to determine the causality between vehicle use and battery ageing. This study identified that capacity fade is

Abbreviations: BEV, battery electric vehicle; BTMS, battery thermal management system; CC-CV, constant current - constant voltage; DOD, depth of discharge; EIS, electrochemical impedance spectroscopy; EV, electric vehicle; G-NMC, graphite – lithium-nickel-manganese-cobalt-oxide; HP, high-performance; HP-C, high-performance-cycle; HP-EV, high-performance electric vehicle; IECC, IEC 62660 – dynamic discharge profile A for BEV cycle test; LIB, lithium ion battery; NMC, lithium-nickel-manganese-cobalt-oxide; OCV, open circuit potential; OEM, original equipment manufacturer; PMC, pulse-multisine characterisation; p-OCV, pseudo-OCV; SEI, solid-electrolyte-interface; SOC, state of charge; WLTP, worldwide harmonised light vehicle Test procedure

* Corresponding author.
E-mail addresses: q.kellner@warwick.ac.uk (Q. Kellner), james.marco@warwick.ac.uk (J. Marco).

https://doi.org/10.1016/j.est.2018.07.018
Received 30 May 2018; Received in revised form 10 July 2018; Accepted 31 July 2018

primarily related to temperature and time, and impedance rise is primarily related to the current profile and the maximum current delivered by the battery. Omar et al. [10] used the cycle life tests defined within the International Standard IEC 62660-1 [11] and ISO 12405-2 [12] to determine the cycle life of a cell intended for passenger vehicle use. Further, Dubarry et al. utilised a dynamic stress test, described within [13], in a cycle life evaluation to determine the rate of change and nature of battery degradation within a passenger vehicles [14,15], providing further evidence that battery degradation is a function of usage profiles.

The authors assert that the nature of high-performance electric vehicle (HP-EV) use cases when compared to driving on public roads is fundamentally different. Previously established testing procedures for cell and battery systems are insufficient to evaluate the suitability of LIB cells (in terms of: cycle life, thermal behaviour, and progression of degradation) for use in evaluation battery technology for HP-EVs [16].The authors' previous work [17] demonstrated significant differences between the "Dynamic discharge profile A for BEV cycle test" as described in the IEC 62660-1 standard, and a newly developed duty-cycle representing HP scenarios. Whilst the IEC standard serves to represent a cell profile for BEVs operating on the road, the high-performance duty cycle (HP-C), in contrast, is representative of an HP-EV driving on a race circuit and was derived from a database of race circuit driving simulations. The validity of the HP-C was assessed against one representative example - the Bahrain International Circuit. This assessment was undertaken using comparative measures based on the duty-cycle design criteria and a thermal simulation.

The derived HP-C has facilitated further engineering activities that are key to successful battery system design and integration. Recently, the authors investigated the differences in thermal behaviour of large format pouch cells subject to the HP-C and IEC standard [18]. The results show that HP scenarios result in higher temperatures and temperature gradients across the cell surface, suggesting increased degradation and localised ageing over prolonged use. Worwood et al. [19] demonstrated that due to the aggressiveness of the HP-C, more involved and unconventional cooling strategies are required for the battery thermal management system (BTMS) to ensure the cells remain within acceptable thermal limits (operating temperature between circa 15–35℃ [20] and maximum temperature gradient of 5 ℃ [21]). Specifically, for cylindrical cells [19], internal cooling with an inserted heat pipe system and/or double tab cooling strategies were required to limit the maximum cell temperature gradient to 5℃, where conventional radial surface cooling gave rise to temperature gradients exceeding 15 ℃. Other experimental studies for pouch cells [22] have also demonstrated the need for more advanced cooling materials to avoid the evolution of thermal gradients exceeding 10 ℃ when exposed to the HP-C. Hosseinzadeh et al. [23] developed a 1D electrochemical-thermal model to simulate the heat generation a 53 Ah pouch cell at various ambient temperatures. In their study a cell was subject to the HP-C, and a profile derived from the WLTP (Worldwide Harmonised Light Vehicle Test Procedure) Class 3 to validate the model and predict the increase in cell temperature arising from these vastly different automotive use cases.

Despite these recent publications assessing battery thermal behaviour when a cell is electrically loaded with a cycle derived from a HP test case, experimental data regarding continuous operation under HP has not been reported within the literature. To better understand and quantify the longer-term impact of such HP-Cs, the next step is to undertake a prolonged experimental study to characterise cell performance and expected life for the HP-EV market.

The research presented within this study extends that published in [17] and provides two key contributions to the body of literature within this field. Primarily, an ageing and characterisation study is conducted to investigate the possible effects and consequences of continuous HP cycling on the electrical characteristics of a 53 Ah pouch cell of G-NMC chemistry (Graphite - Lithium-Nickel-Manganese-Cobalt-Oxide). Within the experimental study, two test groups of cells are subject to continuous cycling using the HP-C and IEC standard profiles to identify the rate and nature of changes in cell behaviour, identified through regular characterisation of the cells during electrical cycling. Prior to this, the validity of the HP-C is refined through an experimental assessment, specifically with regard to the instantaneous electrical behaviour and heat generation of a large format pouch cell.

The paper is structured as follows. Section 2 describes the cell selection process, experimental set-up, HP duty-cycle definitions, and testing methodology. A detailed description of the characterisation tests used to quantify cell parameters is provided. Section 3 presents and discusses the results from the initial cell characterisation, duty cycle validation, and short-term duty-cycle degradation study. Section 3.4 further discusses the results of the cycling study and implications for battery system design for HP vehicle applications, and future testing requirements. Further work and conclusions are presented in Section 4 and 5, respectively.

2. Experimental assessment of cell performance and ageing

Experimental work was undertaken to initially refine the validity of the HP-C developed in [17], and subsequently to characterise large format XALT Energy® 53 Ah NMC pouch cells with regards to its thermal performance and cycle-life. In this section, cell selection, experimental rig design and assembly, cycle choice and methodology is discussed.

2.1. Cell selection

The cells selected are large format pouch cells with G-NMC chemistry at a rated C/2 capacity of 53 Ah (196 Wh); key cell parameters are listed in Table 1. The cell format features a larger surface area-to-volume ratio compared to cylindrical cells and as such, the cell is described by the manufacturer as having better heat dissipation. According to the manufacturer, the cells target high energy applications such as energy storage for HEVs and EVs, grid storage, marine vessels, and locomotives. The combination of high power capability, low internal resistance and higher heat dissipation capability compared to cylindrical cells makes this cell a suitable candidate for HP-EV applications.

2.2. Experimental rig

An experimental rig was designed to facilitate this research. Due to the intensity of the employed testing profiles, an active cooling system was required to keep cells within their thermal safety window. As such the requirement for the experimental rig was to provide a suitable housing for a cooling system, and to facilitate a means of connecting individual cells to a battery cycler.

The experimental rig was modelled using the commercially available software Solidworks. A computer drawing of the test rig is

Table 1
Cell characteristics.

Performance Characteristics	Typical Value (2016)
Capacity at C/2	53 Ah
Nominal Voltage	3.7 V
Discharge Energy (C/2)	196 Wh
Weight	1.15 kg
DC Resistance (10 s @ 50% SOC)	1.33 mΩ
Peak Discharge C-Rate (10 s @ 50% SOC)	8.0 C
Upper Voltage Limit	4.2 V
Lower Voltage Limit	2.7 V
Charge Tempertaure Range	0 °C ~ 45 °C
Discharge Temperature Range	−20 °C ~ 60 °C
Cell Dimensions (LxWxT)	225 × 225 × 11.8 mm

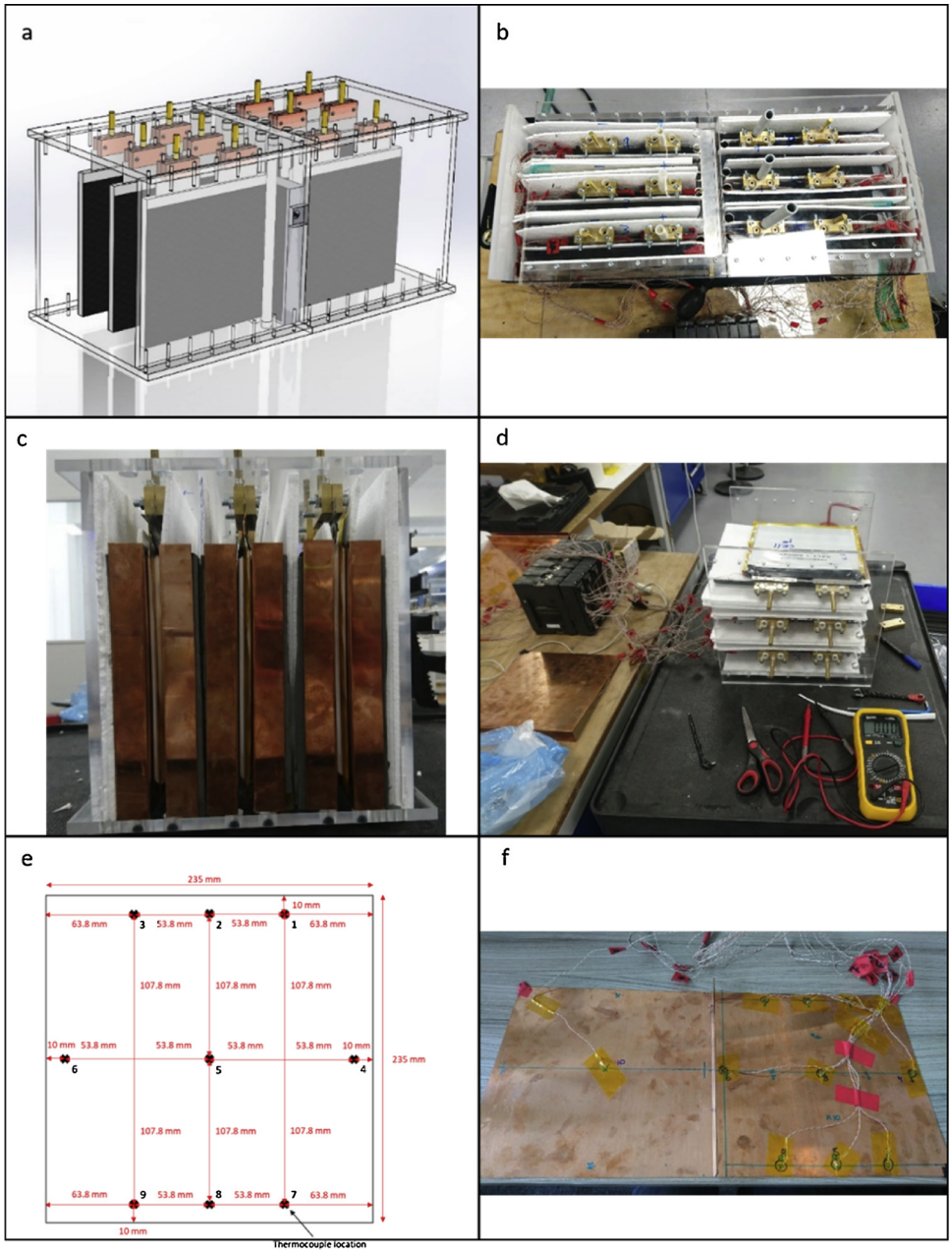

Fig. 1. Test rig design process illustration; a) Test rig CAD model b) Top view of the assembled experimental rig; c) Front view of half rig with bent cooling plates; d) FOAMGLAS® and polystyrene packing of gaps between cells; e) Positions of thermocouples; f) Instrumented cooling fins.

Table 2
Test rig components dimensions.

Component	Height (mm)	Length (mm)	Thickness (mm)
Aluminium cooling plate	210	250	30
Copper cooling fin (fin-cell body)	220	235	0.52
Copper cooling fin (fin-plate contact patch)	220	25	0.52

provided in Fig. 1a, a picture of the completed assembly is shown in Fig. 1b, the dimensions of components are tabulated in Table 2 for reference. A description of its design features, as well as an outline of the assembly process is provided below.

The test rig comprises two Perspex casings, housing a total of 6 cells and an external cooling system.

In each casing, three pouch cells are suspended by their tabs, clamped between two brass blocks which serve as the connection terminal for the battery cycler. The cooling circuit consist of an aluminium cooling plate with internal ducts and a Lauda Thermostat, with the former being located in one of the Perspex casings. The front and back face of each cell are in contact with a pair of L-shaped copper cooling fins. The short edge of each fin is bent at 90° with a radius of 1 mm to form a 25 mm × 210 mm patch as shown in Fig. 1c. These patches are in contact with the aluminium cooling plate, thus providing a means of heat extraction from the testing assembly by means of single edge fin cooling. Space between cooling fin faces of adjacent cells is filled with slabs of polystyrene and FOAMGLAS®, resulting in a densely packed layered structure, thereby ensuring good thermal contact between the cooling fins and cell surface, as shown in Fig. 1d. The FOAMGLAS® slabs are incompressible and enable even pressure to be applied along the length of the cooling fin edge onto the cold plate via

hand tightened ratchet straps. Each pair of cooling fins is instrumented with 10 T-type thermocouples connected to a *"HIOKI® 8423 HiLogger"*. Of the thermocouples, 9 are placed on the fin contacting the front face of a cell, and 1 on the fin contacting the back. This serves to investigate the development of cell temperature and thermal gradients during cell cycling. Fig. 1e shows a schematic of the thermocouple locations for the front facing fin, with a pair of instrumented fins photographed in Fig. 1f. Given the good contact between the cooling fins and the cell surface, the thermocouple measurements are used as pseudo-cell surface measurements [22]. Each cell is individually connected to cell cycling channels, which can provide a maximum current of 400 A per cell. A data acquisition system with a sample frequency of 10 Hz is employed for measuring cell voltage and current.

2.3. Cycle selection

The full derivation of the HP-C is outside the scope of this work and is discussed, in detail, within [17]. However, a brief description is given below.

A database of HP duty-cycles was created by means of simulations using the commercially available software suite *"IPG CarMaker"*. Twelve internationally recognised race circuits of various length, location, and race class were modelled based on satellite imagery. A battery electric sports vehicle was modelled based on the mechanical attributes of the Audi R8 demonstration vehicle that is made available within the software. Key subsystems such as suspension, hydraulic brakes and steering remained unchanged.

However, the conventional powertrain model (e.g. the internal combustion engine and transmission) was replaced with a new model of the electrical machines and battery system. Key subsystem parameters, such as power and torque ratings, and subsystem efficiencies are fully defined within [17]. The vehicle's performance characteristics are detailed in Table 3 and are comparable to those of a conventionally powered vehicle in the same market segment. Finally, a closed-loop driver model was parameterised in terms of aggressiveness with respect to longitudinal and lateral vehicle dynamics to optimise lap times over each circuit. The battery power demand for a lap on each circuit was recorded and normalised with respect to the vehicle's peak power capability.

Each resulting dimensionless profile was subsequently analysed in terms of its amplitude spectrum and cumulative distribution function. A mathematical function approximating the mean of the amplitude spectra was determined, as well as a function approximating the mean of all collected cumulative distribution functions. Using these functions, and utilising the frequency-time domain swapping algorithm described in [24], a generic duty cycle was derived which is representative of the database in both, the time and frequency domain.

The cycle used for verification of the HP-C is the Bahrain cycle. It was generated as part of the work presented within [17], and simulates an electric vehicle driving on the Bahrain international race circuit. It represents a HP use case which was not initially included in the database for the HP-C derivation. It is therefore used as a benchmark against which the IEC standard cycle (IECC) and HP-C are compared.

Table 3
HP-EV performance parameters.

Parameter	Value
Vehicle Body	Rigid body
Vehicle mass	1564 kg
Combined motor power	300 kW
Combined motor torque	850 Nm
0–100 km h^{-1}	3.8 s
0–200 km h^{-1}	12.4 s
Top Speed	300 km h^{-1}

2.4. Test methodology

2.4.1. Cell characterisation

A full characterisation of the cells' attributes prior to testing is required to ensure a small spread of variation between individual specimens. The characterisation process employed within this research is defined in Table 4 and discussed below. A full characterisation refers to the entire table, a partial characterisation refers to those tests marked in bold. Implementation of either a full or partial characterisation test is discussed below.

- The discharge energy capacity test, commonly used in cycle aging studies [25,26], determines the amount of electrical energy that can be stored in the cell under defined environmental and loading conditions. A cell is charged using a constant current-constant voltage (CC-CV) procedure at 26.5 A (0.5C) until a cell reaches a maximum potential of 4.2 V, then kept at 4.2 V, until the charging current drops to 2 A (< 0.04C). Subsequently the cell is left at open potential to equilibrate for 1 h before being discharged with a current of 53 A (1C) until the cut-off potential of 2.7 V is reached. The discharge capacity is defined as the energy extracted during the discharge.
- The pseudo-Open Circuit Voltage (p-OCV) test should be conducted at charging or discharging rates of 0.1C or lower [27] and is conducted after the completed discharge test. The cells are left to rest for 1 h, subsequently charged with a current of 2.65 A (0.1C) up to the cells' upper potential limit of 4.2 V, and held there until the charging current drops below 2 A. By regularly carrying out this test during the life of the cell, it allows for the identification and quantification of changes in the electrochemical thermodynamic properties of the cell as discussed within [28].
- The Pulse Multisine Characterisation (PMC) test, first introduced by Widanage et al. [29], is a characterisation test based on a similar principle as the "Hybrid Pulse Power Characterisation" (HPPC) test. The charge sustaining profile of the PMC is created by a superposition of a sequence of pulses with a multisine. The resulting profile approximates the amplitude spectrum of a duty-cycle derived from a real-world driving cycle, and as such is reported to be more representative of the dynamics a cell is exposed to during operation [30]. Similarly, to the HPPC, the voltage response of a cell to this dynamic profile could be used to parameterize an ECM for a number of SOCs. By tracking the changes within these parameters throughout the cycle life of a cell, information may be inferred regarding the rate of impedance rise and therefore cell ageing. The PMC test was employed at 5 different SOCs as indicated in Table 4.
- Electrochemical Impedance Spectroscopy (EIS) is a non-destructive test that enables the parameterisation of battery ECMs, the individual elements of which may be correlated to electrochemical processes within the cell [31]. The test is carried out by applying an AC sinusoidal current of amplitude 2000 mA to the cell in a frequency range from 10 mHz to 10 kHz, and recording the cell response, from which the cell impedance may be calculated. The use of EIS testing is required as the PMC test is only capable of determining the cell response to inputs at low frequencies (< 10 Hz). From Table 4, the EIS test was carried out at different SOCs, and a rest period of at least 4 h, as is recommended by Barai et al. [31], was employed to allow the dynamics of the cell to stabilise before measurements were made. The tests were carried out on a "*Solartron EnergyLab XM*" and results analysed using "*Scribner® ZView2*".

2.4.2. HP-C validation

Building upon the work presented in [17], in which the HP-C was validated based on profile characteristics and thermal simulations, this test serves to provide further experimental data for validation of the methodology. Emphasis is placed on energy throughput and cell temperature data, as those are often identified as key contributors to cell

Table 4
Characterisation Tests. Tests in bold constitute partial characterisation tests during duty-cycle degradation study.

Assessment Test	Description	SOC	C-Rate
Discharge energy capacity	**Standard test to determine the discharge capacity of every cell**	**100-0%**	**1C**
Slow charge capacity/ p-OCV Test	**Slow charge/p-OCV test. Can be used for DQ/DV analysis**	**0-100%**	**C/10**
PMC Test	A characterisation test to characterise an equivalent circuit model, similarly to the HPPC test capturing nonlinear cell behaviour	**10%, 20%, 50%, 80%, 95%**	**max 7.5C discharge (equipment limited), max 2C charge (cell limited**
EIS Test	Used to investigate the behaviour of the cell. Response can be used to infer degradation mechanisms	**10%**, 20%, **50%**, 80%, **95%**	

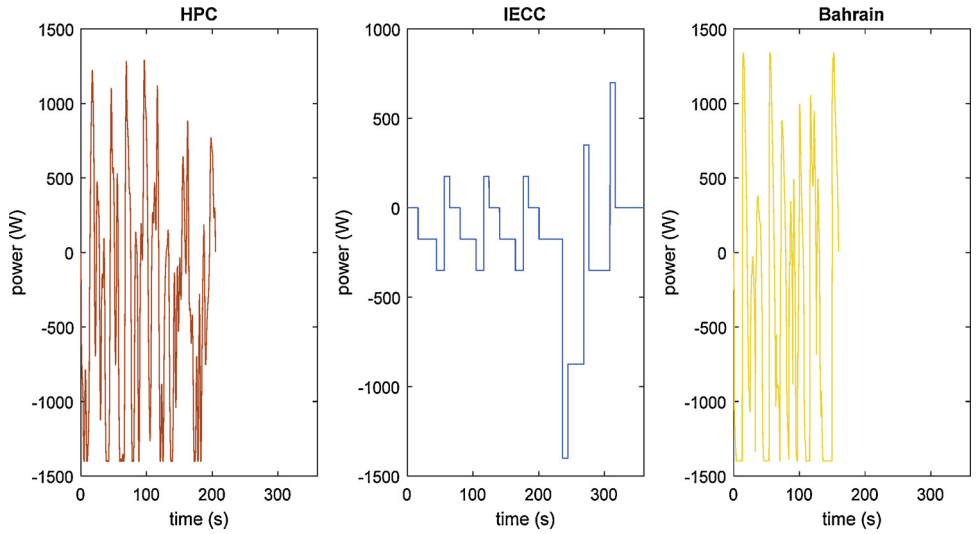

Fig. 2. Selected duty cycles for testing left to right: HP duty-cycle, IEC, Bahrain duty-cycle.

degradation [32] and are known to greatly influence cell performance. Six cells were tested using three different duty cycles, as shown in Fig. 2: The HP-C as described above, the IECC, taken from [11] and a duty-cycle simulating the power demand of an HP-EV driving on the Bahrain International circuit (Bahrain), which was also used for simulation based validation of the HP-C within [17]. Peak power per cell was defined as 1400 W. Negative values of power represent cell discharging, whereas positive values represent charging.

Cells were charged using a CC-CV protocol, followed by a rest period of 1 h. They were then discharged to 95% SOC at 0.5C, followed by another 1 h rest period. Subsequently the cells were subjected to repetitions of a duty cycle, until they either reached a SOC of 10%, resulting in a 45.05 Ah charge depletion, or the peak cell surface temperature reached the thermal safety limit of 65 °C (defined by the manufacturer). Charging currents during testing were limited to 106 A per cell (defined by the manufacturer), and discharging currents were limited to 400 A as per test-equipment limitation.

2.4.3. Duty-cycle degradation study

To assess the longer-term effects of HP-cycling on LIBs, two sets of three cells each were tested simultaneously. Cells No. 1-3 were cycled using the HP-C, whereas cells No. 4-6 were cycled using the IECC, the sets are thus referred to as the HP-C Group and IECC Group, respectively. Following full characterisation (defined in Table 4), cells underwent 200 cycles with regular partial characterisations in between. A cycle within this context refers to a single completion of the protocol used for the HP-C validation described above, followed by a 2 h rest period for cells to cool. Partial characterisation tests were employed to detect whether any effect on the cells' attributes could be observed. Once each cell completed 200 cycles, a full characterisation test was once again undertaken. The complete test schedule is summarised in Table 5.

Table 5
Test program for short term cycling study.

Number of cycles	Total cycles	Test
0	0 (start of test)	Full characterisation
10	10	Partial characterisation
10	20	
10	30	
20	50	
20	70	
20	90	
20	110	
40	150	
50	200 (end of test)	Full characterisation

3. Results and discussion

3.1. Initial characterisation

The energy capacity of all six cells for a 1C discharging and 0.1C charging rate is shown in Fig. 3. The mean discharging capacity is 52.01 Ah with a standard deviation of 0.29 Ah. For the charge capacity test at 0.1C the mean charging capacity is 51.47 Ah with a standard deviation of 0.38 Ah. The measurement spread between the cells for charging and discharging capacity falls within 0.7% and 0.6%, respectively. As currents of different magnitude were used for the capacity tests, the measured capacity between charge and discharge varies. The lower charging current of 0.1C results in lower polarisation and thermal losses during charging, compared to the higher discharging current of 1C. Although the Capacity is measured in Ah and is larger for the higher discharging current, the total amount of energy transferred into the cell (measured in Wh) is larger for the lower current, as illustrated within the tables included in the Fig. 3.

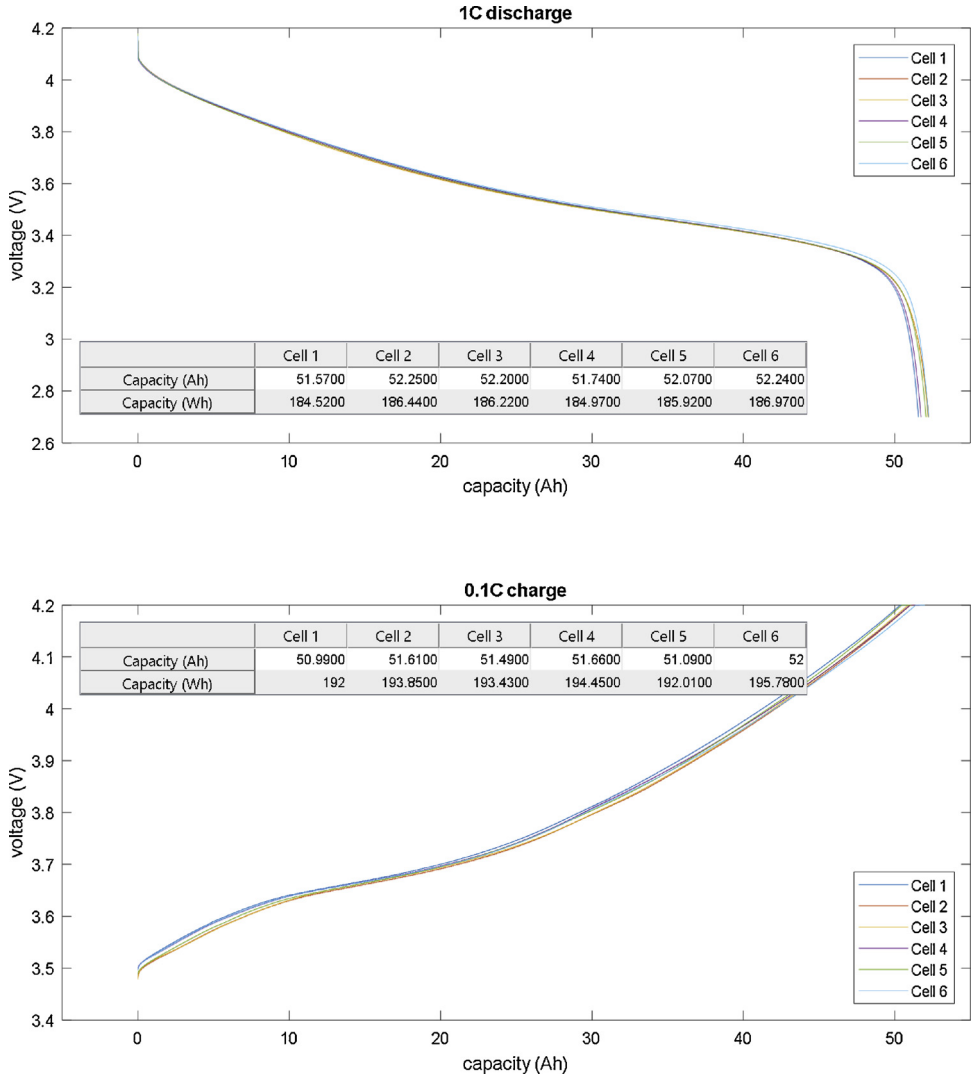

Fig. 3. Capacity test results.

Fig. 4a shows the Nyquist plot for initial EIS characterisation for cell No 4. The imaginary part of the impedance is plotted on the y-axis, and the real part of the impedance is plotted on the x-axis. Fig. 4b displays the variation between cell attributes for 50% SOC, with other SOCs showing a similar spread. The EIS response was fitted to the ECM at the bottom of the figure. The intersection of the inductive trail with the real axis corresponds with the pure Ohmic resistance (R_{0-EIS}), the local minimum of the semicircle in the mid-frequency region, which is associated with the charge transfer resistance (R_{ct-EIS}) corresponds with the values of $R_{1-EIS} + R_{2-EIS}$.

Fig. 4(a–c) shows the fitted ECM parameters for those cells under the PMC for a single RC pair ECM. For the PMC, the voltage response is measured 0.1 s after the electrical current input is applied, as the maximum data sampling frequency of the equipment is 10 Hz. As such, it is not possible to measure responses at higher frequencies and therefore the use of a 2nd order ECM in this instance is not appropriate. The data points represent the mean value for all six cells, and the error bars the standard deviation from the mean. R_0 is defined as the resistance associated with the initial voltage change if a current is applied to a cell, and R_1 is associated with the continual voltage response as charge transfer and diffusion phenomena dominate the cell dynamics.

For the PMC tests, values for R_0 are higher than those found for the EIS tests by a factor of up to 2. This observation is attributed to the maximum sampling frequency of the test equipment utilised [33]. This corresponds to a real impedance of 1.3 m Ω in Fig. 4a. As such, these values correspond better with the mid-frequency measurements from the EIS test. The small spread of both, PMC and EIS values, respectively shows that there is little variation between individual cells at the beginning of testing.

3.2. HP cycle validation

Fig. 5 shows the duty cycle profile, voltage response, and cell surface temperature development for an 85% depth of discharge (DOD) on cell No. 4 for the HP-C, IECC, and Bahrain duty-cycle from left to right, respectively. This cell was chosen as all installed thermocouples operated without interruption throughout the duration of all tests, and as such provides the most reliable thermal test data. Table 6 lists the mean time taken for each duty cycle (∅ time), and the mean energy throughput (∅ Wh) for the set of cells with the associated standard deviation (σ) for each measure. Whilst the HP-C takes 1406 s to complete with an absolute energy throughput of 230 Wh, the IECC requires 122% longer duration with a 13% lower energy throughput and the Bahrain cycle is 42% shorter with only a 9% lower energy throughput. It is clear that the IECC lacks the dynamic behaviour, which both the HP-C and Bahrain cycle exert on the cells. As the HP-C is aimed to be representative of a variety of HP duty cycles and the Bahrain cycle is only a single example of the target use case, the differences between

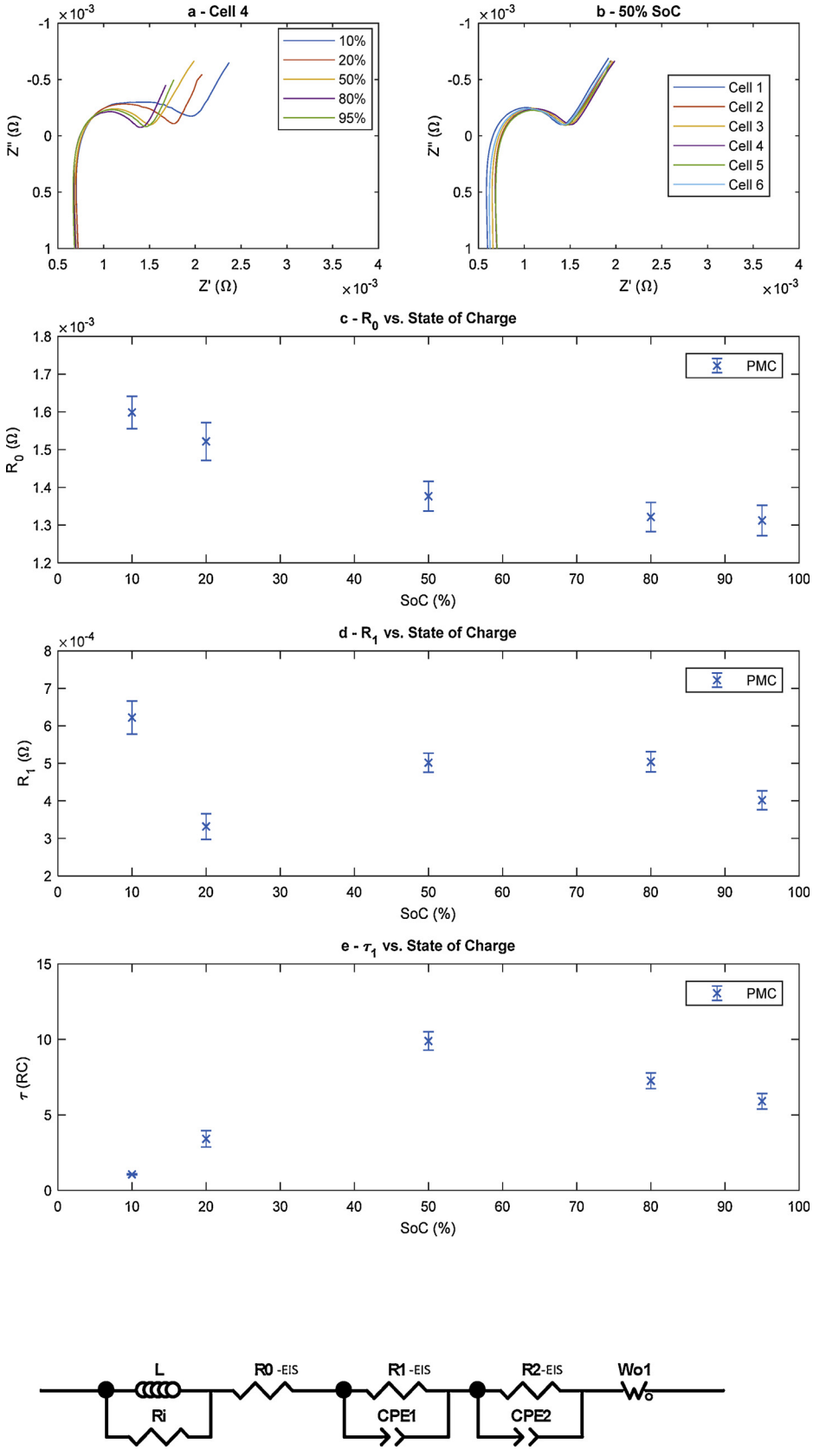

Fig. 4. a EIS plots for cell 4 across defined SOCs; b – EIS plot for all cells at 50% SOC ; PMC – ECM characterisation results for d – R0, e – R1, and f - τ_1; ECM for EIS plot parameterization.

these two cycles with regards to duration and energy requirements are deemed acceptable.

The vast differences in intensity of the HP-C and Bahrain duty-cycle compared to the IECC is further illustrated in the three bottom sub-graphs in Fig. 5, showing the measured cell surface temperatures during discharge for cell No. 4, and Table 7 listing the mean peak temperatures (∅ peak °C) for the hottest and coldest part of the cells, and the peak temperature differences across the cell surface for each cycle, as well as

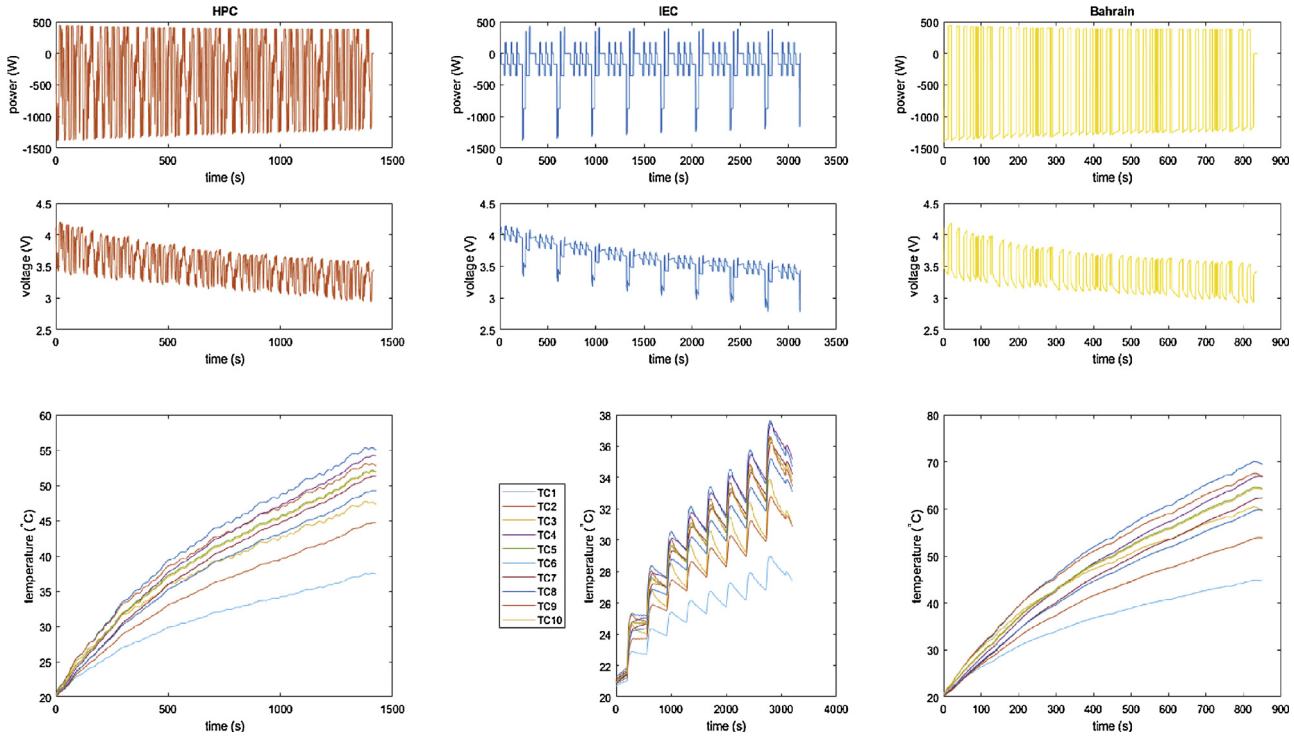

Fig. 5. Duty-cycle profiles, voltage response, and surface temperature development during cycling for cell No. 4 during a discharge from 95-10% SOC: HP duty cycle, IECC, Bahrain (left to right).

Table 6
mean duration of the discharge for each duty cycle, mean energy throughput and the associated standard deviation for each measure for the set of cells.

Cycle	∅ time(s)	σ time	∅Wh throughput	σ Wh
HP-C	1406.1	0.4	230.18	0.73
IECC	3121.1	0.0	199.41	0.52
Bahrain	826.0	0.1	209.49	0.95

Table 7
mean peak temperatures of the hotspot, coldspot, and gradients for the set of cells.

Cycle	∅ peak °C hotspot	σ	∅ peak °C coldspot	σ	∅ peak surface °C gradient	σ
HP-C	54.00	1.56	36.75	0.93	17.24	1.97
IECC	36.93	0.66	28.40	0.81	8.34	0.71
Bahrain	67.30	1.99	43.24	1.76	24.06	2.53

one standard deviation (σ) for each measure. The hotspot on every cell is generally measured on the thermocouple placed at the edge of the cell furthest away from the cooling plate (Pos. 4 – see Fig. 1b). The position underneath the tab, which is furthest away from cooling (Pos. 1), experiences similar temperatures. This, however, is not the always the case, when Pos. 1 displays marginally hotter temperatures than Pos. 4. This observation may be a feature of individual cells, as reported within [34] or, alternatively, attributed to uneven pressure distribution across the cell surface arising from an uneven surface of the polystyrene and FOAMGLAS® slabs, the swelling of cells during cycling, or a shift in position of the thermocouples. The cold-spot of the cell is always measured on the edge of the cell, located closest to the cooling plate in Pos. 6.

Stemming from the intensity of the HP-C and Bahrain duty-cycle reach much higher peak temperatures compared to cycling with the IECC. The hotspots for the IECC reach similar temperature levels to the cold-spots for the HP-C yet are almost 7 °C below the cold spot of cells undergoing the Bahrain cycle. Surface temperature gradients for the IECC reached a mean of 8.34 °C across the cell samples, whereas the surface gradients of the HP-C and Bahrain cycle were 200% and 300% of that value respectively.

Increased cell temperatures in excess of 45 °C have long been identified as a key contributor to accelerated cell degradation, due to accelerated growth of the passivating solid-electrolyte interface (SEI) layer at the anode and increased rate of undesired side reactions as reported within [35–37]. Furthermore, temperature gradients within cells through the central plane have been reported to also contribute to accelerated degradation [38,39]. Parts of the cell at elevated temperatures are expected to have a lower resistance, allowing more current to flow through it, in turn heating up more via a positive feedback process between unique layers that are electrically connected in parallel, and localised parts in the same layer. This in turn may lead to localised aging, and accelerate the ageing process [40]. To conduct realistic cycle life studies the choice of a testing profile which results in representative cell self-heating is therefore of paramount importance. As such, from a thermal perspective, it may be argued that within the HP use case, international testing standards such as IEC 62660-1/2 and ISO 12405-1/2 are inadequate for evaluating cycle life and thermal design requirements and that the presented HP-C offers a more realistic target profile.

3.3. Duty-cycle study

Fig. 6 presents for both, the HP-C Group and IECC Group, the progression of cell capacity retention against the cells' energy throughput from HP-C and IECC cycling, respectively, throughout the duty-cycle degradation study, as measured during each partial characterisation test. The discharge capacity extracted from the 1C discharge tests is shown in the top two graphs, the charge capacity, determined during C/10 charging is shown in the bottom two graphs. The data points represent the mean of each group, with the error-bars measuring one standard deviation. Both, the discharge and charge capacity increases throughout testing for both test groups. The initial and final charging

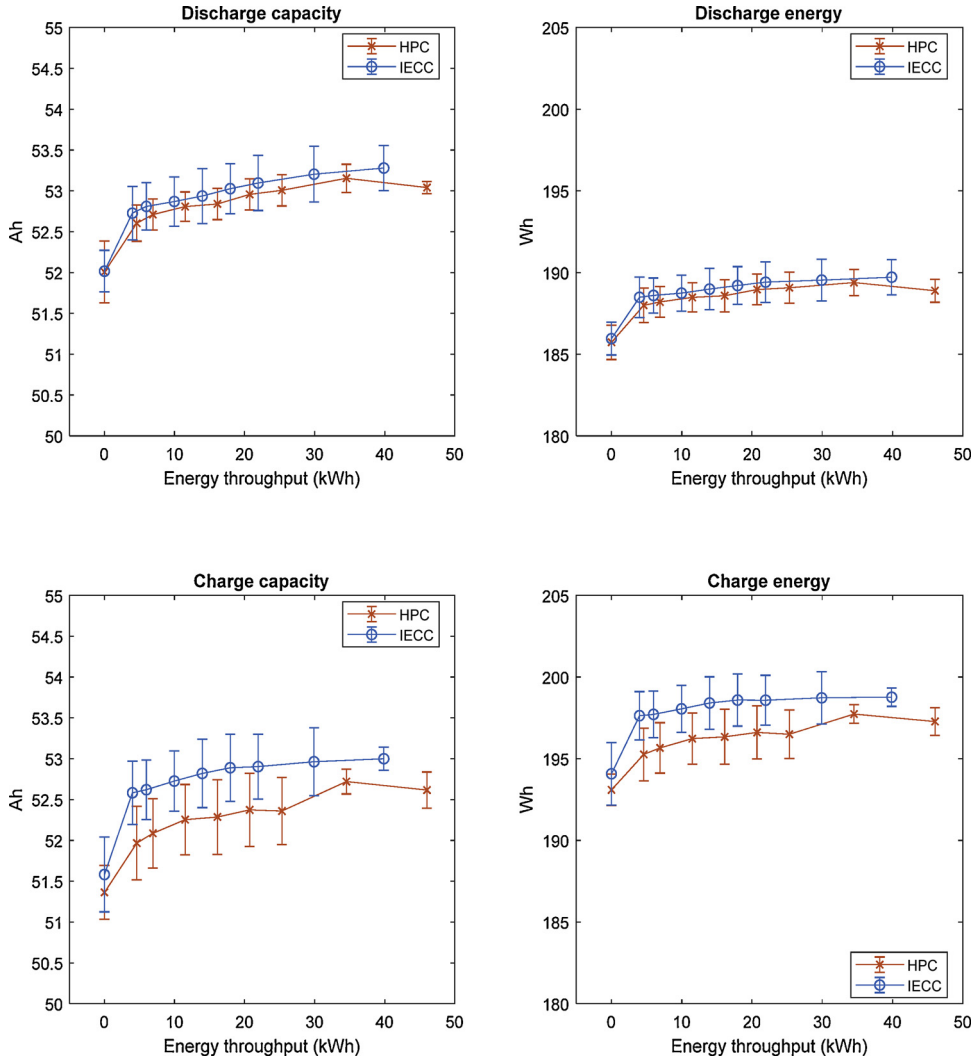

Fig. 6. Cell capacity throughout testing at characterisations.

Table 8
Charge and discharge capacity for the HP-C and IECC test groups.

	Initial Ah	Final Ah	Δ %	Initial Wh	End Wh	Δ %
IECC (discharge)	52.02	53.28	2.42	186.00	189.70	1.99
HP-C (discharge)	52.01	53.04	1.98	185.70	188.90	1.72
IECC (charge)	51.58	53	2.75	194.10	198.80	2.42
HP-C (charge)	51.36	52.62	2.45	193.10	197.30	2.18

and discharging capacities for both test groups, and the calculated change (Δ) are tabulated in Table 8.

The highest measured capacity for the HP-C group is at 53.15 Ah (189.4 Wh), in the penultimate characterisation, before reducing to 53.04 Ah (188.9 Wh) at the final characterisation, whereas the IECC group's capacity is still steadily increasing. However, the capacity measurements of the HP-C group are within the error of the previous measurement and overlap with the error of the IECC group. From the capacity measurements alone, no definitive start of capacity fade can be asserted from the experimental data.

Increases in cell capacity at the early stages of cycling for cells of similar chemistry and format have been reported within [41] and [42]. Jalkanen [41] et al. tested 3 Dow Kokam®[1] 40 Ah pouch at room temperature, 45 °C and 65 °C for continuous 1C charge and discharge cycling. All three cells initially have a higher discharge capacity than the nominal capacity declared by the manufacturer, and capacity increases to a maximum, before decreasing. Based on the presented results, the cell discharged at 45 and 65 °C reach their maximum capacity within the first 100 cycles, the cell cycled at room temperature reaches a first peak at around 200 cycles and a second at 500 cycles. The rate of subsequent decrease in capacity is fastest for the cell cycled at 65 °C, which gave a shorter cycle life than the other two cells.

De Hoog et al. [42] tested EIG® 20 Ah NMC pouch cells to formulate a model which separates calendar and cycle ageing. They observed an initial increase in cell capacity for calendar ageing and combined calendar and cycle ageing tests, an effect which was more pronounced for cells stored at low states of charge, and subject to lower DOD.

Both studies explained their observations with a process referred to as electrochemical milling. During charge and discharge electrodes expand and contract, resulting in internal stresses, which in the case of non-uniform stress distribution within the electrode may result in micro-cracks forming in the electrode material, exposing fresh sites and pathways for lithium ion intercalation [43]. This in turn causes a widening of the of the operating voltage window of the electrodes, the extent of which can be determined using reference electrode tests. Provided parasitic side reactions are minimal, and fractured particles maintain good electronic contact, this may result in increased capacity and reduced internal resistance. Cracking in electrode material can be

[1] Dow Kokam rebranded to XALT Energy

caused by high currents and high DOD. Both duty cycles tested reach c-rates exceeding 7.5C, making electrode cracking a possible pathway for changes in the electrode particles and as such the capacity increase observed in both test groups within this work may also be correlated to the onset of electrochemical milling.

Another possible explanation for the capacity increase observed within this study is a potential gradual decrease in external pressure applied to the cells over time. As the cells are densely packed at the beginning of cycling, continual cycle testing, and the associated expansion and contraction of cells may lead to deformations in the packed polystyrene slabs that will in turn reduce the lateral force on the cells. Barai et al. [44] reported a decrease of cell capacity coupled with an increase in impedance for NMC pouch cells which had an external pressure applied to them. They observed a 2% capacity decrease for an external pressure of 0.8 bar. The authors assert that a pressure difference of 0.8 bar resulting from deformed polystyrene slabs is unlikely. Furthermore, a change of this magnitude would result in significantly worse, and observable cell cooling nearer the end of the duty-cycle degradation study. However, no such observation could be made within the recorded data. As such, the more plausible cause of capacity increase is that of electrochemical milling. However, it is noteworthy that based on the capacity test data alone, without further observations from within the cells themselves, it is not possible to make a definitive conclusion.

Graphs for differential capacity analysis for both test groups are presented in Fig. 7. The curves show the derivatives of the charge vs. voltage (dQ/dV) curves recorded for the 0.1C charge for the p-OCV test, with the area under the curve equating to the energy capacity of the cell. The upper subplots show the results for both test groups at the initial and final characterisation tests, respectively. The lower subplots present a direct comparison between the initial and final characterisations for the HP-C and IECC groups, respectively. An advantage of these plots is that changes in the p-OCV and voltage vs. capacity plots can be seen more easily. The underpinning theory behind the analysis of these graphs is discussed in detail in [15,28,45,46].

Based on the Initial characterisations, three regions of interest were investigated and displayed in magnified areas within Fig. 7a–c. The features of the curves displayed in the initial characterisation graph are explained as follows. At 0% SOC, the graphite electrode is almost completely delithiated. During charging, Li^+ ions intercalate into the graphite layers and the material transitions through several phases as the lithium content within the material increases [47,48]. One of these phase transitions is indicated in the peak around a full cell potential of 3.52 V in Fig. 7a, in which a wide spread of peak height can be observed within the cells in terms of the height of the dQ/dV peak. Cells No. 2 and 3 display the most pronounced peak whilst Cell No.1's peak is least defined.

At the beginning of charge, the NMC electrode material is almost fully lithiated in a hexagonal O3 layered structure [49]. During charge, as lithium is extracted, a phase change occurs from the hexagonal to a monoclinic lattice [50], manifesting in the peak identified in Fig. 7b around a cell potential of 3.66 V. Similarly, to the peak in Fig. 7a, a wide spread of peak height can be observed for the test groups. Cells No. 6, 4 and 1 have the three highest peaks, respectively, with the remaining cells showing similar behaviour. Between 3.75 V and 4.2 V NMC then displays a steady potential with the material in the solid-solution region. The third region of interest is located at the beginning of charge in Fig. 7c. All 6 cells display a similar OCV between 3.46 V and 3.48 V. However, the initial dQ/dV values vary significantly.

Comparing the observations of the initial full characterisation to the results displayed for the final full characterisation, significant differences may be observed. Firstly, by comparing Fig. 7a with d, the intensity of the peak in the latter appears to have increased whilst the spread of intensity between cells has been greatly reduced. The increase in area underneath this peak indicates that a larger amount of energy capacity may be attributed to the phase change process associated with the graphite electrode compared to initial measurements. The order of peak intensity as seen for the initial characterisation test has also changed, with the HP-C group having slightly lower peak intensity than the IECC group. Furthermore, a shift in the peak position toward the lower cell potential is observed, which is associated with a shift to a lower impedance within the cell [45]. By examination of Fig. 7g the peak for the HP-C group after 200 cycles shifted approximately 10 mV from 3.53 V to 3.52 V, whereas the shift for the IECC group (Fig. 7k) is slightly larger at 20 mV from 3.53 V to 3.51 V.

Secondly, by comparing Fig. 7b and e, a smaller spread in peak height for final characterisation tests can be seen, but no clear trend in height gain or reduction for either the HP-C (Fig. 7h) or IECC (Fig. 7l) group. Whilst cells No. 1, 4 and 6 show a decrease in peak height, cells No. 2 and 5 show an increase, and no significant change can be observed for cell No 3. However, a horizontal shift of the peaks toward higher cell potentials is observed, with the shift of the HP-C group being slightly larger, which may indicate a higher internal resistance.

Thirdly, linking region f) to region c), a significant change in the starting OCV is observable with a mean shift of 85 mV for the HP-C group (Fig. 7j), and a mean shift of 63 mV for the IECC group (Fig. 7m) toward a lower potential, in conjunction with a lower spread in initial dQdV values for both test groups. Inspection of Fig. 7f and j also reveal an additional peak at a potential of 3.45 V. Based on the information provided within [47,48], this new peak is most likely resulting from a phase change in the earlier lithiation process of the graphite electrode. This decrease of the OCV is directly related to the increase in energy capacity. An increase in the OCV of a cell, as reported by Stiaszny et al. [51], is caused by a reduction in cyclable lithium stemming from the NMC electrode as lithium is irreversibly used in SEI layer formation and growth. The reduced OCV observed in this study thus requires an increase in cyclable lithium.

A possible source for these observations may be minor cracks in the NMC material, providing fresh reaction sites, which previously were not accessible due to diffusion or mass transfer limitations in the electrode particles or porous electrode matrix, respectively. Without reference electrode tests it is not possible to assign definitively the observed changes in the OCV to changes in either the graphite, or NMC electrode, but the current results provide further indication that cells experience electrochemical milling. Further work required to reaffirm this conclusion is presented in Section 4.

Fig. 8(a–c) shows the change in ECM parameters, extracted from the PMC tests of the two test groups during the duty-cycle degradation study. Values for R_0 show an increase from their initial values through to their final characterisation for both test groups with the HP-C group having a slightly higher increase throughout the SOC range. Values for R_1, partially associated with charge transfer and diffusion phenomena, decrease after cycling for SOCs of 50%, 80% and 95%, and show an increase for an SOC of 20%. The increase in R_1 at 20% SOC is linked to the change in peak between 3.5 V and 3.56 V in Fig. 7d. Values for R_1 and τ_1 at 10% SOC have been excluded from the results as the cell lower voltage limit of 2.7 V was reached during characterisation tets.

Fig. 8d and e show the Nyqiuist plots derived from the EIS tests for Cell No. 1 from the HP-C group at the initial characterisation and after 200 cycles, respectively, for a number of SOCs. Fig. 8f and g, show the same Nyquist plots for cell No. 4 from the IECC test group. For both cells, a shift of the intersection of the inductive trail toward higher values of Z' is observed. The position of the local minimum in the midfrequency semicircles, however, does not show any obvious signs of movement from it's original location. The mean values of the pure Ohmic resistance (R_{0-EIS}), as extracted from the Nyquist plots, for the HP-C and IECC groups, is presented in Fig. 8h, with the error bars representing one standard deviation from the mean. Values of R_{0-EIS}, which is attributed to the resistance of the bulk electrode material and electrolyte, show an increase for both test groups throughout the SOC range. This observation is in agreement with the increase for R_0 from the PMC test. It indicates changes in the cell bulk material, likely

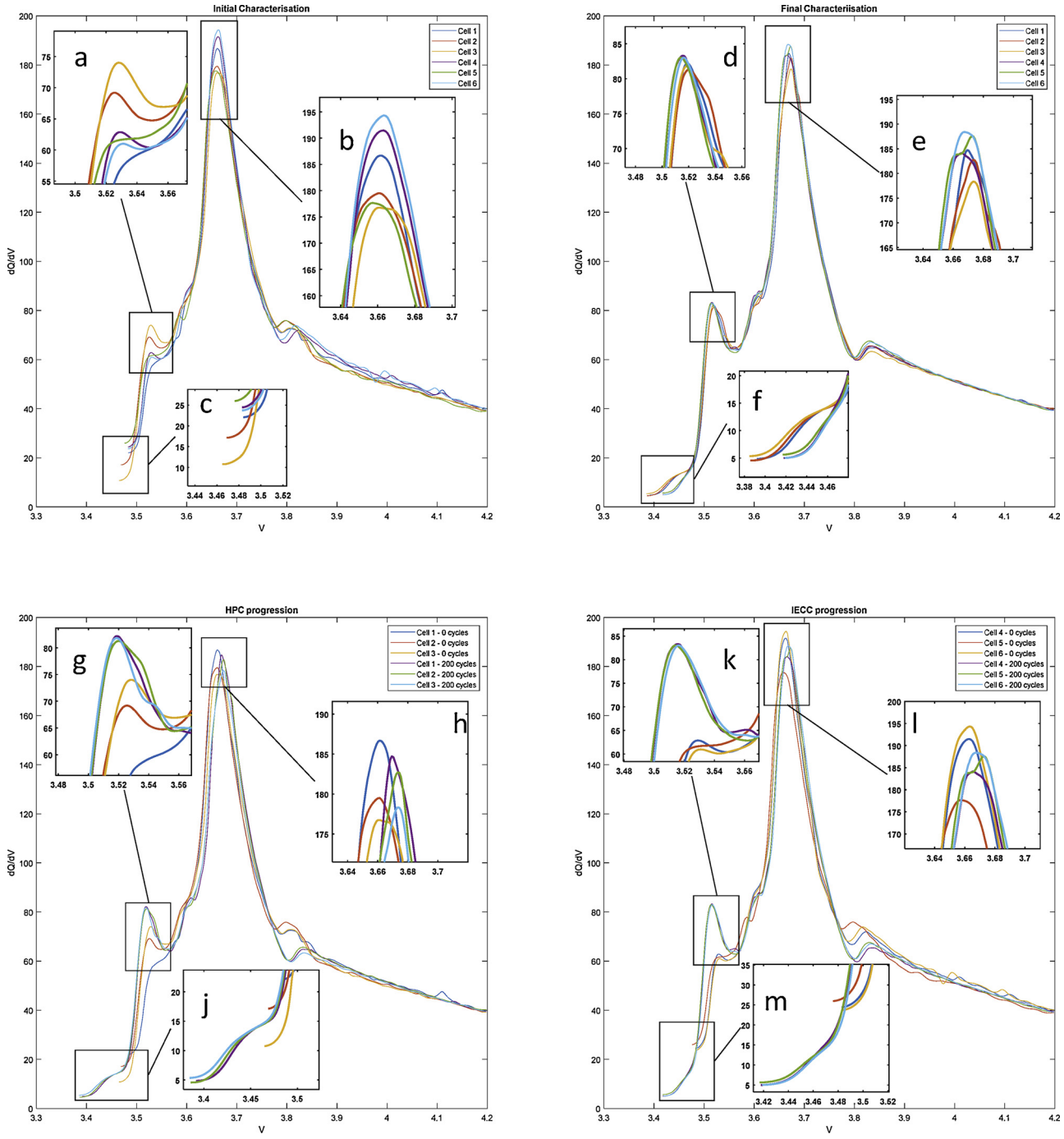

Fig. 7. Incremental Capacity Analysis - top left: Initial Characterisation; top right: final characterisation; bottom left: HP-C cell progression; bottom right: IECC cell progression.

associated with degradation mechanisms, such as potential particle cracking. The values of the charge-transfer resistance, (R_{ct-EIS}), associated with the local minimum of the mid frequency semicircle in the Nyquist plots, show a decrease after the completion of the study, as shown in Fig. 8j. This downward shift is known [31] to be linked to improved transfer kinetics at the electrode electrolyte interfaces in the porous electrode. As discussed within [42,43,52], one reason for this may be an increase in active surface area for Li-ion intercalation which could have been caused by electrode cracking. This shift appears to be of a larger magnitude for the HP-C test sample.

The reduction in charge transfer resistance in combination with the increase in bulk resistance is a further indication that electrochemical milling may be occurring during the test. As previously suggested, the introduction of micro-cracks in the electrode material may allow fresh sites, some of which may have previously been diffusion limited, to be exposed to the electrolyte. This in turn would result in an increased surface area of reaction sites, transfer kinetics, and allow for a greater amount of lithium to be used for cycling reactions, thus providing a plausible explanation for the decrease in R_{ct-EIS}, and increase in cell energy capacity. The increase in bulk resistance in this case is assumed to stem from a degradation of the electrolyte and slightly worsened electrical contact of the electrode material. As high-currents are a known pathway for electrode particle cracking, the higher reduction of R_{ct-EIS} for the HP-C group as shown in Fig. 8j is plausible, as their cycling profile more frequently utilises high currents.

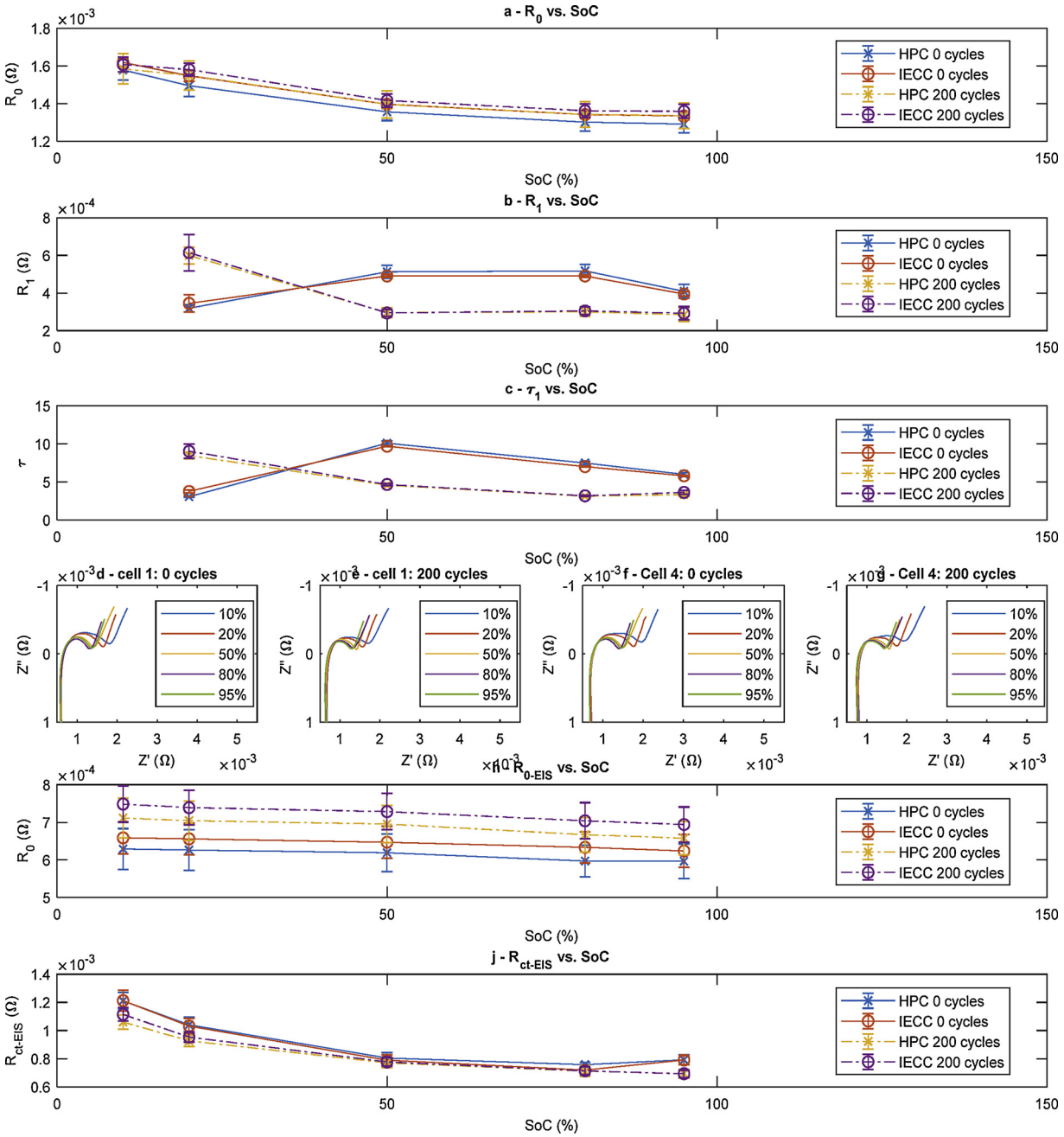

Fig. 8. a–c: progression of ECM parameters as derived from PMC tests for a – R_0; b – R_1; c – τ_1; d – Nyquist plots for cell 1 at beginning of testing; e – Nyquist plot for cell 1 after 200 cycles; f – Nyquist plots for cell 4 at beginning of testing; g – Nyquist plot for cell 4 after 200 cycles; h – mean Ohmic resistance of test groups derived from Nyquist plots, j – mean charge-transfer resistance of test groups derived from Nyquist plots.

3.4. Further discussion on the results of the duty-cycle degradation study

Both test groups show a minor increase in the pure Ohmic resistance, and small decrease in the charge transfer resistance, and an increase in the overall cyclable capacity. At the end of the study (200 cycles) the cells from the HP-C group appear slightly worse off pertaining to impedance rise and capacity retention in direct comparison with the cells from the IECC test group. However, these differences cannot completely be correlated to the aggressiveness of the HP-C cycle profile, as the overall energy throughput of the HP-C group's cells is higher, and the spread of experimental results within both test groups overlap. These observed changes of cell characteristics are likely ascribed to micro-cracking in the electrode material, or electrochemical milling. However, to eliminate any doubt about this assessment, additional testing is required. Initially, a reference electrode test would enable the analysis of the graphite and NMC electrodes separately. Secondly, post-mortem testing, such as X-ray diffraction (XRD) and scanning electron microscopy (SEM) can be used to confirm if micro-cracking is present in electrode materials in their current state. Similar investigations have been reported within [37]. These tests, however, are outside the scope of this initial study.

It is currently not known whether the observations made within this work are solely conditional on the use of high electrical currents, or if the cells are designed to operate in this fashion. Were testing to be continued, it would be expected that, once the cell side reactions overtake the milling effect, the micro-cracking in the cells would cause accelerated degradation over time compared to cells that would not expect this cracking. A possible way to test for this eventuality would be

to cycle a further test group with the same mean current as the HP-C or IECC, but lower peak currents and observe whether an initial energy capacity increase, and charge transfer resistance decrease can be observed, and at which rate this occurs. The authors aim to continue the experimental work and report further results in future articles.

With regards to temperature related behaviour, as previously identified, cells subject to elevated temperatures, and high temperature differences across the cell surface, are known to experience accelerated degradation mechanisms and ageing. Elevated temperatures enable increased parasitic side reactions between the electrolyte and the carbon electrode, leading to increased SEI growth and a reduction in energy capacity. The rate of this degradation is known to follow Arrhenius law [37]. However, at the end of the duty-cycle degradation study within this work, neither the HP-C, nor the IECC group show significant signs of temperature related ageing. Even for the HP-C group, which is exposed to significantly higher temperatures during cycling than the IECC group, no temperature related ageing has yet been observed. Although average cell temperature in the HP-C cells regularly exceeds 40 ^{0}C during cycling, the total duration of these instances is relatively small due to active cooling of the cells during cycling and rest periods, possibly explaining the absence of temperature related degradation indicators. Although no observations of this nature could be made, it is highly likely that, with continued testing, the cells within the HP-C group would show signs of temperature related degradation before the cells in the IECC group.

4. Limitations of the study and further work

The duty-cycle degradation study presented within this work is limited to 200 cycles and cells show only little degradation in their electrical characteristics. The expected degradation sequence has not been observed yet and further testing is required to confirm whether the cells within this study follow a typical degradation profile. As such, the authors recommend continued testing of the cells until their end of useful life (80% retained capacity, 100% impedance increase) can be verified. To confirm the occurrence of micro-cracks in the electrode material, further testing of the cells in their current state is also recommended. Firstly, reference electrode tests can be performed to identify whether the change in cell characteristics are underpinned by changes in the anode or cathode, secondly XRD and SEM tests to check for visible structural changes within the electrode.

The observations and assessments made regarding the cycling study within this work are only valid for the type of cell used, and for the thermal constraints of the tests. The experimental rig set-up was primarily designed to maintain the safe operating temperature of the cells, and to maximise their operating window to further facilitate cell characterisation. As such, its intended use is constrained to experiments within a laboratory environment and in its current form it is not proposed as a vehicle solution for cell thermal management. For these research findings to be applicable to vehicles, a battery thermal management system would be required to extract the same amount of heat from the cells as the experimental rig within this study.

It is noteworthy that the cells are designed for long cycle life and high-power applications as they have a lower energy density and internal resistance than standard automotive cells. Furthermore, the manufacturer of the cells used within this study is a supplier to FIA Formula-E. The effect of HP cycling on batteries with different chemistries and form factors cannot be known without further testing, although testing on standard automotive cells (i.e. higher energy density and internal impedance) would be more likely to show degradation at earlier stages and would reveal the impact of HP scenarios when compared to standard road vehicles. The authors also recommend that the testing procedure within this work is repeated without active cooling efforts to identify the effect of thermal management on the results of the duty-cycle degradation study.

The tests within this work only consider the effects of electrical loading and ignore the harsh vibration environment encountered on race tracks. It is known that vehicle vibrations contribute to the degradation of cells [53,54] and as such a combined testing study with vibration and cycling demands further exploration. Lastly, the effect of AC current ripples, as discussed within [55] in the system during cell operation, as may occur during operation in an EV, is not considered due to the fidelity of the testing equipment.

5. Conclusions

In this work a 53 Ah Graphite-NMC pouch cell was characterised with respect to cell characteristics and cycle life, and a HP duty cycle was validated based on experimental data. By direct comparison of the HP-C with the Bahrain duty cycle and the IECC, it has become evident that the new proposed HP-C is more representative of HP driving scenarios than existing procedures. The disparity between the heat generation within cells during the IECC and the HP-C shows that the use of a representative duty cycle is vital when benchmarking cells for design activities pertaining battery thermal management. The considerable differences in thermal behaviour of the two test cases also underpins the requirement that cycle-life studies employ the HP-C over the IECC to characterise cells for their usable cycle-life in automotive HP scenarios.

During the cycle life study, counterintuitively the cells in both test groups have shown an increase in cyclable energy capacity, a reduction in charge-transfer resistance, and an increase in pure Ohmic resistance. The cells within the HP-C test sample have shown more changes in cell characteristics than those in the IECC group, if only marginal. As such, the cells used within this study can deliver a total of 200 track driving sessions without showing signs of capacity decrease or significant overall impedance rise, provided active cell cooling is present. Although no definitive conclusion can be drawn without further reference electrode testing and destructive SEM and XRD tests, the observations in this work suggest that the changes in cell characteristics are most likely caused by cracking of the electrode material. From a review of the academic literature, the high electrical currents employed within the tests have been identified as a likely source. This in turn indicates future accelerated degradation such as a reduction in energy capacity and impedance rise due to extensive cracking and the associated worsened electrical contact with continued use compared to cells which do not show signs of cracking. The higher frequency of occurrence of high electrical current pulses in the HP-C group compared to the IECC group furthermore suggests that with continued cycling, cells within the HP-C test group will degrade at a faster rate as electrical testing continues.

Temperature dependent degradation effects have not yet been observed within either test group. The higher cell temperatures, and surface temperature differences observed in the HP-C test group suggest that, with continued use, accelerated capacity loss and impedance rise due to faster SEI growth may also be observed compared to the IECC cells.

The findings within this study provide an insight into the evolution of cell characteristics during use within a HP use case, and highlights the limitations in the understanding of cell degradation in this area. Furthermore, it delivers important information pertaining the thermal management requirements of cells within the automotive HP segment. This research will support further activities regarding the operation and degradation of cells used within HP-EVs.

Acknowledgements

The research presented within this paper is supported by the Engineering and Physical Science Research Council through the awards EP/M507593/1 and EP/I01585X/1. The research was undertaken in collaboration with the WMG Centre High Value Manufacturing Catapult (funded by Innovate UK) in collaboration with Jaguar Land Rover and Delta Motorsport. The authors would like to express gratitude to Jaguar

Land Rover and Delta Motorsport for their advice and support. Data available upon request.

References

[1] Y. Zhou, M. Wang, H. Hao, L. Johnson, H. Wang, H. Hao, Plug-in electric vehicle market penetration and incentives: a global review, Mitig. Adapt. Strateg. Glob. Change (2014), https://doi.org/10.1007/s11027-014-9611-2.

[2] Aston Martin News, Aston Martin Confirms Production of First All-electric Model, (2017).

[3] D. Deng, Li-ion batteries: basics, progress, and challenges, Energy Sci. Eng. 3 (2015) 385–418, https://doi.org/10.1002/ese3.95.

[4] J. Groot, M. Swierczynski, A.I. Stan, S.K. Kær, On the complex ageing characteristics of high-power LiFePO4/graphite battery cells cycled with high charge and discharge currents, J. Power Sources 286 (2015) 475–487, https://doi.org/10.1016/j.jpowsour.2015.04.001.

[5] Y. Zhang, C.Y. Wang, X. Tang, Cycling degradation of an automotive LiFePO4 lithium-ion battery, J. Power Sources 196 (2011) 1513–1520, https://doi.org/10.1016/j.jpowsour.2010.08.070.

[6] X. Han, M. Ouyang, L. Lu, J. Li, Y. Zheng, Z. Li, A comparative study of commercial lithium ion battery cycle life in electrical vehicle: aging mechanism identification, J. Power Sources 251 (2014) 38–54, https://doi.org/10.1016/j.jpowsour.2013.11.029.

[7] Y. Zhang, C.-Y. Wang, Cycle-life characterization of automotive lithium-ion batteries with LiNiO[sub 2] cathode, J. Electrochem. Soc. 156 (2009) A527, , https://doi.org/10.1149/1.3126385.

[8] M. Safari, C. Delacourt, Aging of a commercial graphite/LiFePO4 cell, J. Electrochem. Soc. 158 (2011) A1123, , https://doi.org/10.1149/1.3614529.

[9] A. Barré, F. Suard, M. Gérard, M. Montaru, D. Riu, Statistical analysis for understanding and predicting battery degradations in real-life electric vehicle use, J. Power Sources 245 (2014) 846–856, https://doi.org/10.1016/j.jpowsour.2013.07.052.

[10] N. Omar, P. Van Den Bossche, G. Mulder, M. Daowd, J.M. Timmermans, J. Van Mierlo, S. Pauwels, Assessment of performance of lithium iron phosphate oxide, nickel manganese cobalt oxide and nickel cobalt aluminum oxide based cells for using in plug-in battery electric vehicle applications, 2011 IEEE Veh. Power Propuls. Conf. (2011) 1–7, https://doi.org/10.1109/VPPC.2011.6043017.

[11] International Electrotechnical Commission, IEC 62660-1, (2010).

[12] BSI Standards Publication (2012), BS ISO 12405-2:2012 Electrically Propelled Road Vehicles—Test Specification for Lithium-ion Traction Battery Packs and Systems, (2012).

[13] Idaho National Laboratory, U. S. Department of Energy Vehicle Technologies Program Battery Test Manual For Plug-In Hybrid Electric Vehicles - Revision 3, U.S. Dep. Energy. (2015) 16–18.

[14] M. Dubarry, V. Svoboda, R. Hwu, B.Y. Liaw, Capacity and power fading mechanism identification from a commercial cell evaluation, J. Power Sources 165 (2007) 566–572, https://doi.org/10.1016/j.jpowsour.2006.10.046.

[15] M. Dubarry, B.Y. Liaw, Identify capacity fading mechanism in a commercial LiFePO4 cell, J. Power Sources 194 (2009) 541–549, https://doi.org/10.1016/j.jpowsour.2009.05.036.

[16] Q. Kellner, W. Dhammika Widanage, J. Marco, Battery power requirements in high-performance electric vehicles, 2016 IEEE Transp. Electrif. Conf. Expo, IEEE, Dearborn, MI, USA, MI, USA, 2016, pp. 1–6, , https://doi.org/10.1109/ITEC.2016.7520194.

[17] Q. Kellner, E. Hosseinzadeh, G. Chouchelamane, W.D. Widanage, J. Marco, Battery cycle life test development for high-performance electric vehicle applications, J. Energy Storage. 15 (2018) 228–244, https://doi.org/10.1016/j.est.2017.11.019.

[18] Q. Kellner, D. Worwood, W.D. Widanage, J. Marco, Electrical and thermal behavior of pouch-format lithium ion battery cells under high-performance and standard automotive duty-cycles, 2017 IEEE Veh. Power Propuls. Conf., IEEE (2017) 1–5, https://doi.org/10.1109/VPPC.2017.8330865.

[19] D. Worwood, Q. Kellner, M. Wojtala, W.D. Widanage, R. McGlen, D. Greenwood, J. Marco, A new approach to the internal thermal management of cylindrical battery cells for automotive applications, J. Power Sources 346 (2017) 151–166, https://doi.org/10.1016/j.jpowsour.2017.02.023.

[20] G.K.A. Pesaran, S. Santhanagopalan, Addressing the impact of temperature extremes on large format Li-ion batteries for vehicle applications, 30TH Int. Batter. Semin. (2013).

[21] A. Pesaran, Battery thermal models for hybrid vehicle simulations, J. Power Sources 110 (2002) 377–382, https://doi.org/10.1016/S0378-7753(02)00200-8.

[22] D. Worwood, Q. Kellner, E. Hosseinzadeh, D. Mullen, D. Greenwood, J. Marco, R. McGlen, K. Lynn, D. Mullen, R.M. Glen, E. Hosseinzadeh, D. Mullen, D. Greenwood, J. Marco, R. McGlen, K. Lynn, Thermal analysis of fin cooling large format automotive lithium-ion pouch cells, 2017 IEEE Veh. Power Propuls. Conf., IEEE (2017) 1–6, https://doi.org/10.1109/VPPC.2017.8330874.

[23] E. Hosseinzadeh, R. Genieser, D. Worwood, A. Barai, J. Marco, P. Jennings, A systematic approach for electrochemical-thermal modelling of a large format lithium-ion battery for electric vehicle application, J. Power Sources 382 (2018) 77–94, https://doi.org/10.1016/j.jpowsour.2018.02.027.

[24] J. Schoukens, T. Dobrowiecki, Design of broadband excitation signals with a user imposed power spectrum and amplitude distribution, IEEE Instrum. Meas. Technol. Conf. (1998), pp. 1002–1005.

[25] E. Sarasketa-Zabala, I. Gandiaga, E. Martinez-Laserna, L.M. Rodriguez-Martinez, I. Villarreal, Cycle ageing analysis of a LiFePO4/graphite cell with dynamic model validations: towards realistic lifetime predictions, J. Power Sources 275 (2015) 573–587, https://doi.org/10.1016/j.jpowsour.2014.10.153.

[26] C. Pastor-Fernández, T. Bruen, W. Widanage, M. Gama-Valdez, J. Marco, A study of cell-to-cell interactions and degradation in parallel strings: implications for the battery management system, submitted for publication, J. Power Sources 329 (2016) 574–585, https://doi.org/10.1016/j.jpowsour.2016.07.121.

[27] C. Pastor-Fernández, K. Uddin, G.H. Chouchelamane, W.D. Widanage, J. Marco, A comparison between electrochemical impedance spectroscopy and incremental capacity-differential voltage as Li-ion diagnostic techniques to identify and quantify the effects of degradation modes within battery management systems, J. Power Sources 360 (2017) 301–318, https://doi.org/10.1016/j.jpowsour.2017.03.042.

[28] M. Dubarry, V. Svoboda, R. Hwu, B. Yann Liaw, Incremental capacity analysis and close-to-equilibrium OCV measurements to quantify capacity fade in commercial rechargeable lithium batteries, Electrochem. Solid-State Lett. 9 (2006) A454, , https://doi.org/10.1149/1.2221767.

[29] W.D. Widanage, A. Barai, K. Uddin, A. Mcgordon, J. Marco, Design and use of multisine signals for Li-ion battery equivalent circuit modelling. Part 1: Signal design, Submitt. to J. Power Sources (under Rev. 324 (2015) 1–25. doi:https://doi.org/10.1016/j.jpowsour.2016.05.014.

[30] W.D. Widanage, A. Barai, G.H. Chouchelamane, K. Uddin, A. McGordon, J. Marco, P. Jennings, Design and use of multisine signals for Li-ion battery equivalent circuit modelling. Part 2: model estimation, J. Power Sources 324 (2016) 61–69, https://doi.org/10.1016/j.jpowsour.2016.05.014.

[31] A. Barai, G.H. Chouchelamane, Y. Guo, A. McGordon, P. Jennings, A study on the impact of lithium-ion cell relaxation on electrochemical impedance spectroscopy, J. Power Sources 280 (2015) 74–80, https://doi.org/10.1016/j.jpowsour.2015.01.097.

[32] J. Vetter, P. Novák, M.R. Wagner, C. Veit, K.-C. Möller, J.O. Besenhard, M. Winter, M. Wohlfahrt-Mehrens, C. Vogler, A. Hammouche, Ageing mechanisms in lithium-ion batteries, J. Power Sources 147 (2005) 269–281, https://doi.org/10.1016/j.jpowsour.2005.01.006.

[33] A. Barai, K. Uddin, W.D. Widanage, A. McGordon, P. Jennings, A study of the influence of measurement timescale on internal resistance characterisation methodologies for lithium-ion cells, Sci. Rep. 8 (2018) 1–13, https://doi.org/10.1038/s41598-017-18424-5.

[34] T. Grandjean, A. Barai, E. Hosseinzadeh, Y. Guo, A. McGordon, J. Marco, Large format lithium ion pouch cell full thermal characterisation for improved electric vehicle thermal management, J. Power Sources 359 (2017) 215–225, https://doi.org/10.1016/j.jpowsour.2017.05.016.

[35] S.B. Chikkannanavar, D.M. Bernardi, L. Liu, A review of blended cathode materials for use in Li-ion batteries, J. Power Sources 248 (2014) 91–100, https://doi.org/10.1016/j.jpowsour.2013.09.052.

[36] S. Käbitz, J.B. Gerschler, M. Ecker, Y. Yurdagel, B. Emmermacher, D. André, T. Mitsch, D.U. Sauer, Cycle and calendar life study of a graphite|LiNi1/3Mn 1/3Co1/3O2 Li-ion high energy system. Part A: full cell characterization, J. Power Sources 239 (2013) 572–583, https://doi.org/10.1016/j.jpowsour.2013.03.045.

[37] T. Waldmann, M. Wilka, M. Kasper, M. Fleischhammer, M. Wohlfahrt-Mehrens, Temperature dependent ageing mechanisms in lithium-ion batteries—a post-mortem study, J. Power Sources 262 (2014) 129–135, https://doi.org/10.1016/j.jpowsour.2014.03.112.

[38] M. Fleckenstein, O. Bohlen, M.A. Roscher, B. Bäker, Current density and state of charge inhomogeneities in Li-ion battery cells with LiFePO 4 as cathode material due to temperature gradients, J. Power Sources 196 (2011) 4769–4778, https://doi.org/10.1016/j.jpowsour.2011.01.043.

[39] Y. Troxler, B. Wu, M. Marinescu, V. Yufit, Y. Patel, A.J. Marquis, N.P. Brandon, G.J. Offer, The effect of thermal gradients on the performance of lithium-ion batteries, J. Power Sources 247 (2014) 1018–1025, https://doi.org/10.1016/j.jpowsour.2013.06.084.

[40] I.A. Hunt, Y. Zhao, Y. Patel, J. Offer, Surface cooling causes accelerated degradation compared to tab cooling for lithium-ion pouch cells, J. Electrochem. Soc. 163 (2016) A1846–A1852, https://doi.org/10.1149/2.0361609jes.

[41] K. Jalkanen, J. Karppinen, L. Skogström, T. Laurila, M. Nisula, K. Vuorilehto, Cycle aging of commercial NMC/graphite pouch cells at different temperatures, Appl. Energy 154 (2015) 160–172, https://doi.org/10.1016/j.apenergy.2015.04.110.

[42] J. de Hoog, J.M. Timmermans, D. Ioan-Stroe, M. Swierczynski, J. Jaguemont, S. Goutam, N. Omar, J. Van Mierlo, P. Van Den Bossche, Combined cycling and calendar capacity fade modeling of a nickel-manganese-cobalt oxide cell with real-life profile validation, Appl. Energy 200 (2017) 47–61, https://doi.org/10.1016/j.apenergy.2017.05.018.

[43] J. Christensen, Modeling diffusion-induced stress in Li-Ion cells with porous electrodes, J. Electrochem. Soc. 157 (2010) A366, , https://doi.org/10.1149/1.3269995.

[44] A. Barai, Y. Guo, A. Mcgordon, P. Jennings, A study of the effects of external pressure on the electrical performance of a lithium-ion pouch cell, Int. Conf. Connect. Veh. Expo. (2013) 295–299, https://doi.org/10.1109/ICCVE.2013.155.

[45] A.J. Smith, J.R. Dahn, Delta differential capacity analysis, J. Electrochem. Soc. 159 (2012) A290–A293, https://doi.org/10.1149/2.076203jes.

[46] M. Dubarry, C. Truchot, B.Y. Liaw, Synthesize battery degradation modes via a diagnostic and prognostic model, J. Power Sources 219 (2012) 204–216, https://doi.org/10.1016/j.jpowsour.2012.07.016.

[47] V.A. Sethuraman, L.J. Hardwick, V. Srinivasan, R. Kostecki, Surface structural disordering in graphite upon lithium intercalation/deintercalation, J. Power Sources 195 (2010) 3655–3660, https://doi.org/10.1016/j.jpowsour.2009.12.034.

[48] D. Allart, M. Montaru, H. Gualous, Model of lithium intercalation into graphite by potentiometric analysis with equilibrium and entropy change curves of graphite electrode, J. Electrochem. Soc. 165 (2018) A380–A387, https://doi.org/10.1149/2.

1251802jes.
[49] M.M. Doeff, J.B. Goodenough, K. Naoi, K.R. Bullock, Batteries for Sustainability, Springer, New York, 2013, https://doi.org/10.1007/978-1-4614-5791-6.
[50] R. Jung, M. Metzger, F. Maglia, C. Stinner, H.A. Gasteiger, Oxygen release and its effect on the cycling stability of $LiNi_x Mn_y Co_z O_2$ (NMC) cathode materials for Li-Ion batteries, J. Electrochem. Soc. 164 (2017) A1361–A1377, https://doi.org/10.1149/2.0021707jes.
[51] B. Stiaszny, J.C. Ziegler, E.E. Krauß, M. Zhang, J.P. Schmidt, E. Ivers-Tiffée, Electrochemical characterization and post-mortem analysis of aged LiMn 2O4-NMC/graphite lithium ion batteries part II: calendar aging, J. Power Sources 258 (2014) 61–75, https://doi.org/10.1016/j.jpowsour.2014.02.019.
[52] M. Dubarry, C. Truchot, B.Y. Liaw, Cell degradation in commercial LiFePO4cells with high-power and high-energy designs, J. Power Sources 258 (2014) 408–419, https://doi.org/10.1016/j.jpowsour.2014.02.052.
[53] J.M. Hooper, J. Marco, G.H. Chouchelamane, J.S. Chevalier, D. Williams, Multi-axis vibration durability testing of lithium ion 18650 NCA cylindrical cells, J. Energy Storage 15 (2018) 103–123, https://doi.org/10.1016/j.est.2017.11.006.
[54] J.M. Hooper, J. Marco, G.H. Chouchelamane, C. Lyness, Vibration durability testing of nickel manganese cobalt oxide (NMC) lithium-ion 18,650 battery cells, Energies 9 (2016) 1–27, https://doi.org/10.3390/en9010052.
[55] K. Uddin, A.D. Moore, A. Barai, J. Marco, The effects of high frequency current ripple on electric vehicle battery performance, Appl. Energy 178 (2016) 142–154, https://doi.org/10.1016/j.apenergy.2016.06.033.